

**Flexible hybrid piezo/triboelectric energy harvester with high power density  
workable at elevated temperatures**

**Yanhua Sun<sup>a</sup>, Yun Lu<sup>a</sup>, Xiaoning Li<sup>a</sup>, Zheyin Yu<sup>a</sup>, Shujun Zhang<sup>a</sup>, Huajun  
Sun<sup>b</sup>, Zhenxiang Cheng<sup>\*a</sup>**

*<sup>a</sup>Institute for Superconducting and Electronic Materials, Australian Institute for  
Innovative Materials, University of Wollongong, North Wollongong, NSW 2500,  
Australia*

*<sup>b</sup>State Key Laboratory of Silicate Materials for Architectures, Center for Smart  
Materials and Device Integration, School of Materials Science and Engineering,  
Wuhan University of Technology, Wuhan 430070, China*

**Corresponding author:** Zhenxiang Cheng

**\*E-mail:** [cheng@uow.edu.au](mailto:cheng@uow.edu.au)

**Tel:** 61-2-42981406

**Address:** Institute for Superconducting and Electronic Materials, Australian  
Institute for Innovative Materials, University of Wollongong, North  
Wollongong, NSW 2500, Australia

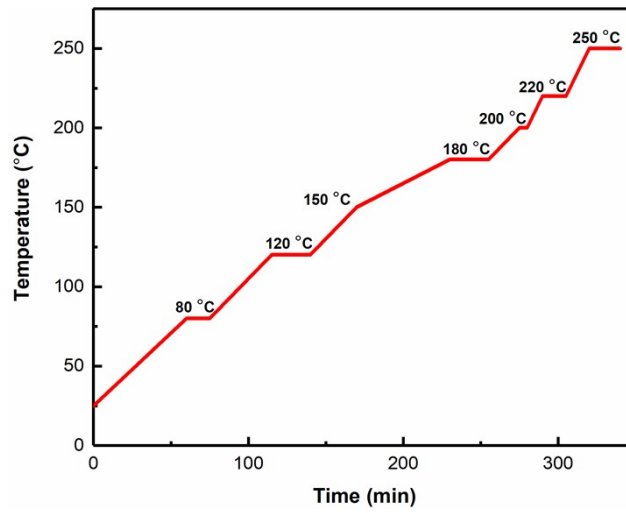


**Fig. S1** Solidification process for the PI and BF-BT/PI film.

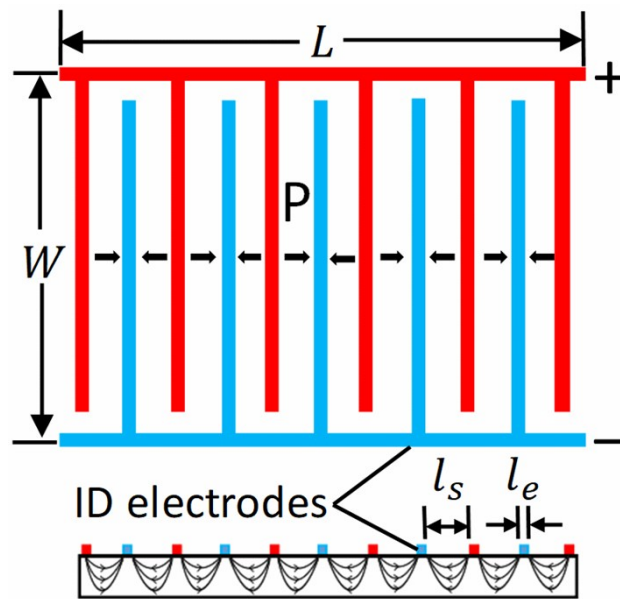


**Fig. S2** Schematic diagram of the device with interdigital (ID) electrodes and the polarization distribution from a cross-sectional view.

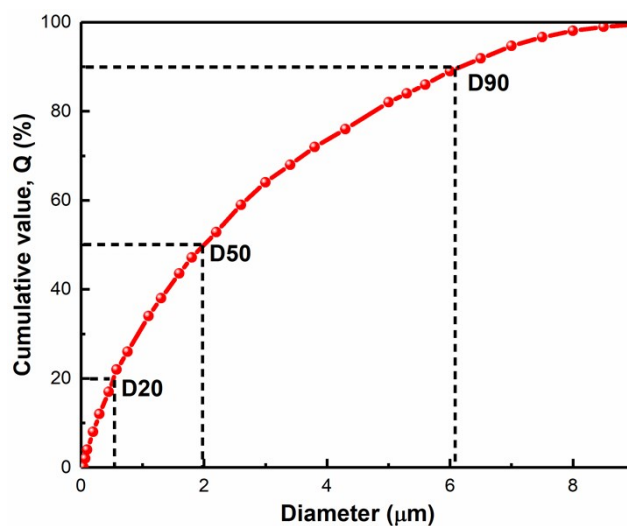


Fig. S3 Diameter distribution of the BF-BT particles.

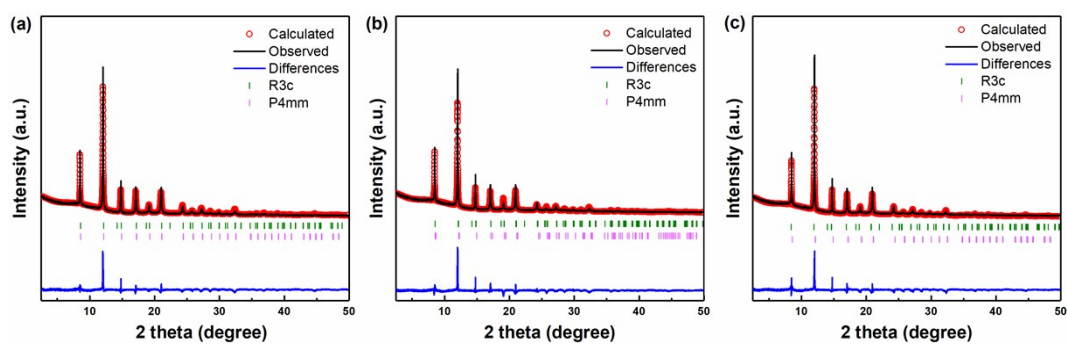
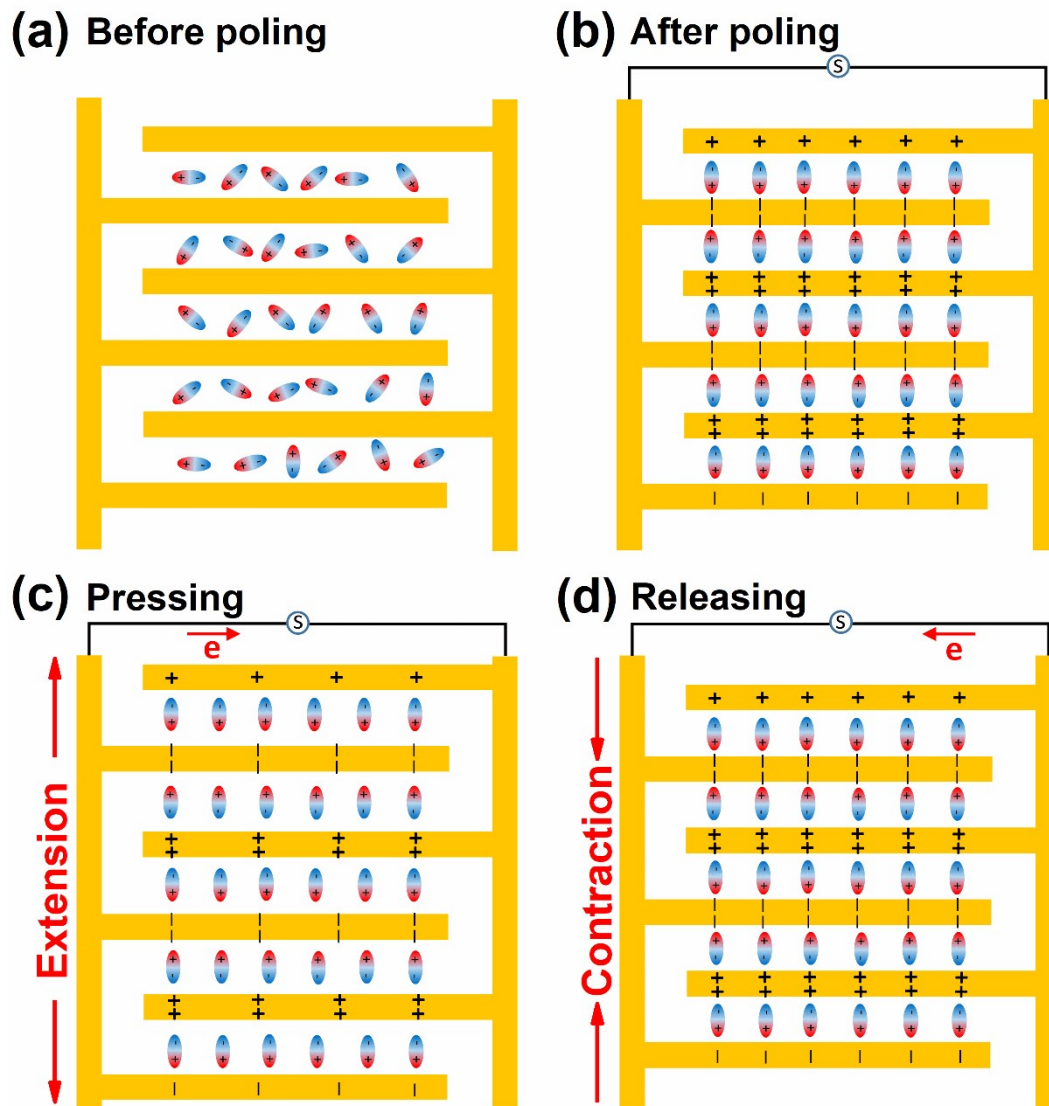


Fig. S4 Synchrotron XRD patterns and refinement results for 0.7BF-0.3BT at (a) 400 K,  $R_{wp} = 8.43\%$ ,  $R_p = 6\%$ , (b) 600 K,  $R_{wp} = 8.62\%$ ,  $R_p = 5.96\%$ , (c) 700 K,  $R_{wp} = 8.94\%$ ,  $R_p = 6.19\%$ .



**Fig. S5** Schematic illustration of dipole alignment during the poling and pressure application process: i) Dipoles in BF-BT particles are randomly aligned before the poling process. ii) After poling, the dipoles in the BF-BT particle will align in the direction along the electric field. iii) When a compressive force is applied on the PEH, a piezoelectric potential is generated. iv) As the compressive force is released, the accumulated electrons flow back in the opposite direction.

As shown in **Fig. S5(a)**, the ferroelectric domains are aligned randomly in the BF-BT within the PI matrix prior to the poling process. After applying a strong electric field on the device, the ferroelectric domains tend to align in the direction of electric field, as shown in **Fig. S5(b)**. The rearranged domains maintain a permanent polarization (remanent polarization) even after the removal of the poling voltage, which is the source of their high piezoelectric potential with

respect to an external force. In the original state, the device is not subjected to an external force, and there is no output electric signal because of electrical equilibrium. When a vertical compressive force is applied on the PEH device, the changed distance between two finger electrodes will lead to a change in the total polarization of the composite between the two electrodes, which results in a positive and negative piezoelectric potential change, respectively. Therefore, the free charges gathered at the electrodes will flow through the external circuit to balance the piezoelectric potential. As a result, an electric pulse will be generated in responding to the mechanical stress. Furthermore, when the external pressure on the PEH device is removed, the distance between two neighbouring electrodes will recover to the original state, and thus the piezoelectric potential will disappear. Consequently, the free electrons accumulated at the electrode flow back, which can generate a negative electrical signal. The continuous application and release of the external force on the PEH device will generate repetitive positive and negative electrical pulses.<sup>[1, 2]</sup>

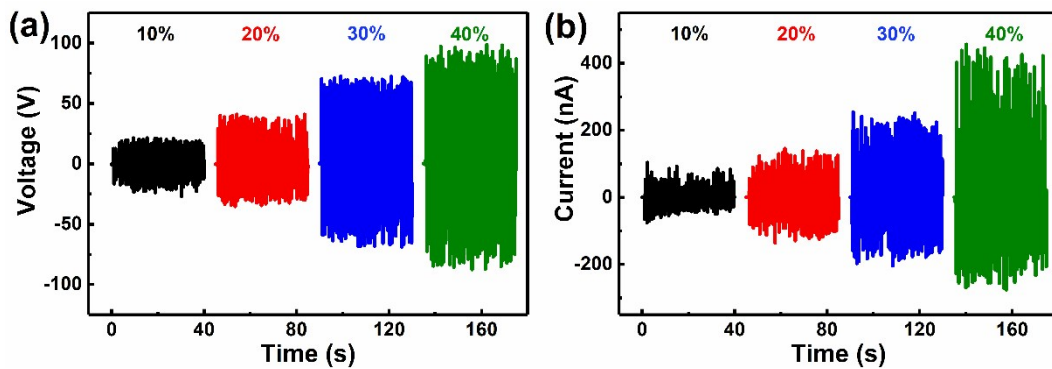


**Fig. S6** (a-b) Time-dependent open circuit voltage and short-circuit current for fabricated PEHs with 10-40% BF-BT weight fractions.

**Fig. S6** show the typical time-dependent short-circuit currents and open-circuit voltages for the various PEHs under cyclic pressing and releasing processes, with the same pressure of  $\sim 0.18$  MPa and frequency of  $\sim 1$  Hz. The output open-circuit voltage and short-circuit current increase significantly with increasing mass fraction of BF-BT powder, output open-circuit voltages

around 24, 41, 72, and 101 V and short-circuit currents around 100, 140, 250, and 460 nA can be obtained from PEHs with BF-BT particles fractions of 10, 20, 30, and 40 wt%, respectively.

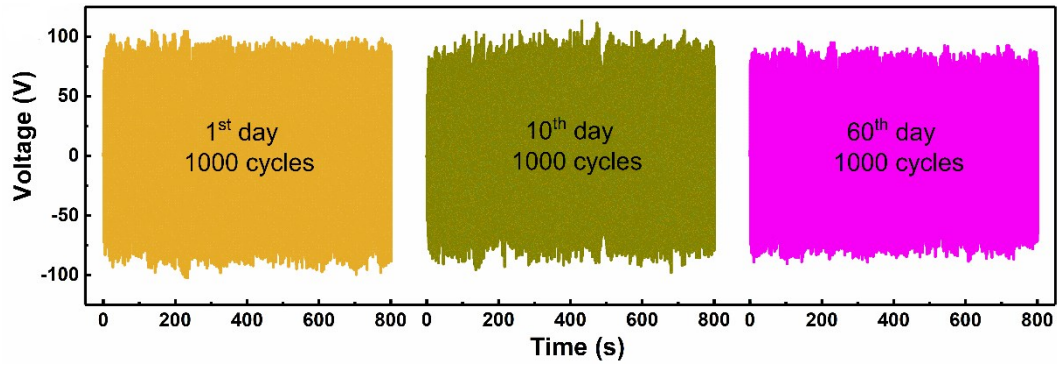


**Fig. S7** The results of a punching durability test carried out 1000 times for a PEH measured at three different periods after poling, after 1 day, 30 days, and 60 days.

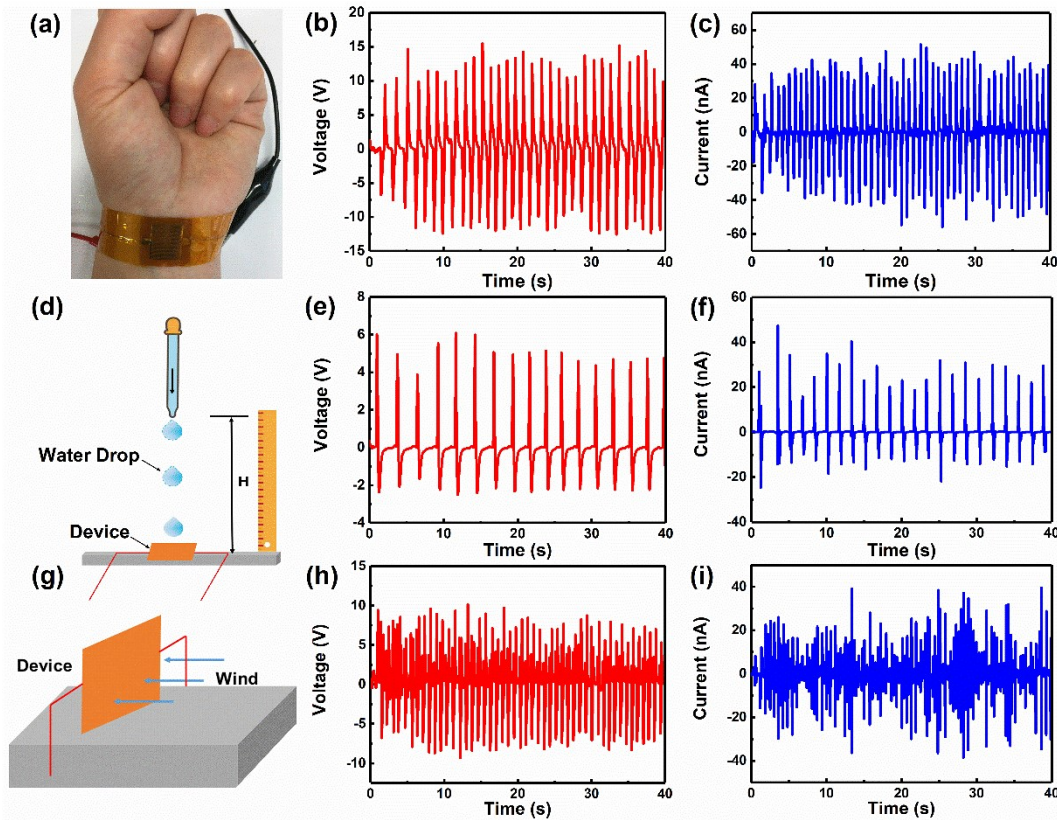


**Fig. S8** Sensor measurement results: Open circuit voltage and short circuit current when a PEH with 40% BF-BT was used as a sensor: (a-c) bent by wrist movement; (d-f) sensing the fall of drops of water; and (g-i) sensing blowing wind.

Besides having outstanding energy harvesting performance, the flexible PEHs respond sensitively to human motion and changes in the external environment, such from as wrist bending, the fall of drops of water, and blowing wind. **Fig. S8a-c** presents the open-circuit output voltage and short-circuit current from the PEH device with 40 wt% BF-BT particles during human motion when a single device is attached to the wrist joint. In response to a slight movement of the wrist, a peak voltage of 15.5 V and current of 55 nA were produced, respectively, which is much higher than the previously reported results.<sup>[3, 4]</sup> Furthermore, as shown in **Fig. S8d-f**, an impact was introduced by the fall of drops of water with a mass of 0.1 g from a height of 30 cm. The force applied on the device by the water drops can be calculated by the formula  $\Delta mgh/\Delta t$ , where  $\Delta mgh$  is the momentum change of the water drop, which is assumed to be totally transferred to the PEH device, and  $\Delta t$  is the interaction time of the water drop on the device.  $\Delta mgh$  is calculated as  $mgh$  after the water drop is completely stopped on the device, where  $m$  is the weight of the water drop,  $g$  is the acceleration due to gravity, and  $h$  is the dropping height. The impact time is assumed according to the width of the output signal of the device, which is about 0.2 s. Therefore, the force applied on the device by the dropping water is approximately  $1.5 \times 10^{-3}$  N when the dropping height is 30 cm. The flexible device responds actively to the tiny impact with an open circuit voltage of 6 V and short circuit current of 47 nA. In the case of sensing blowing wind, the device is set up vertically on a bread board and subjected to continuously blowing air at a speed of about 8 m/s, where the maximum output voltage and current were detected to be 10 V and 39 nA (**Fig. S8g-i**), respectively. The fairly large response of the flexible PEH device to the human motion, water drops, and blowing air clearly indicates its capability for sensing or harvesting not only biomechanical energy, but also environmental energy due to its splendid sensitivity and flexibility.

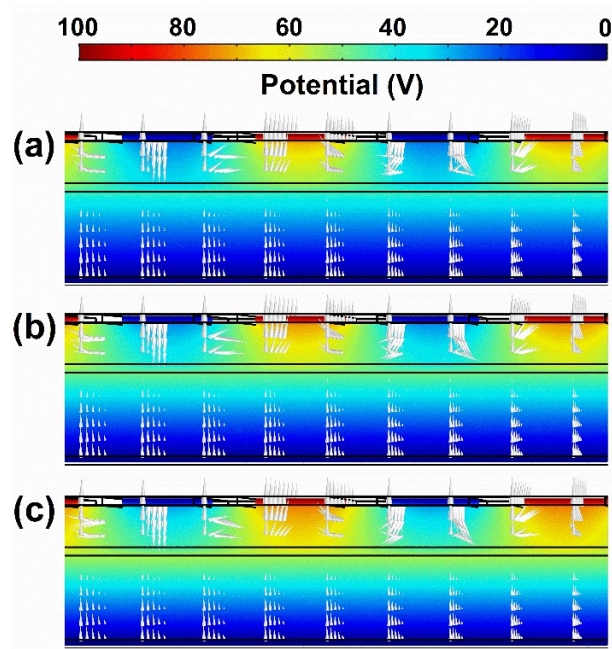


**Fig. S9** Consol simulation of electric potential distribution of the PEH when combined with TEH with (a) 5  $\mu\text{C}/\text{m}^2$ , (b) 10  $\mu\text{C}/\text{m}^2$  and (c) 15  $\mu\text{C}/\text{m}^2$  surface charge density.

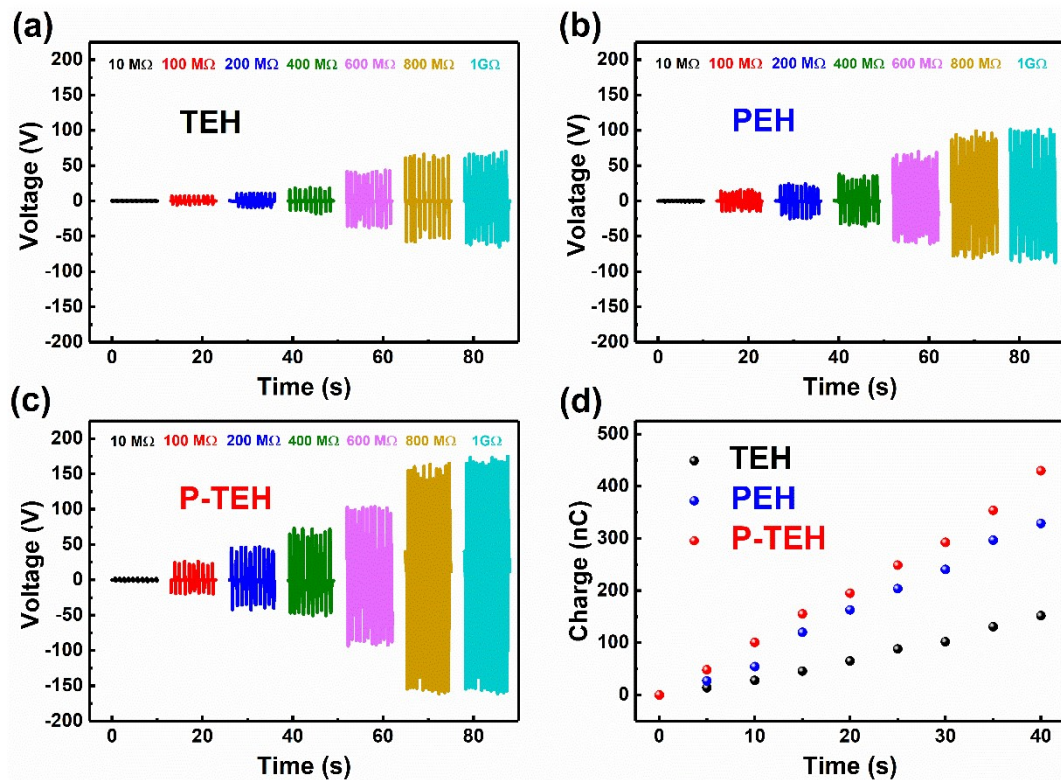


**Fig. S10** Output voltage of (a) TEH, (b) PEH, and (c) P-TEH measured under different external resistance loadings in the range from 10  $\text{M}\Omega$  to 1  $\text{G}\Omega$ . (d) Charges generated by the TEH, PEH, and P-TEH under the continuous tapping.



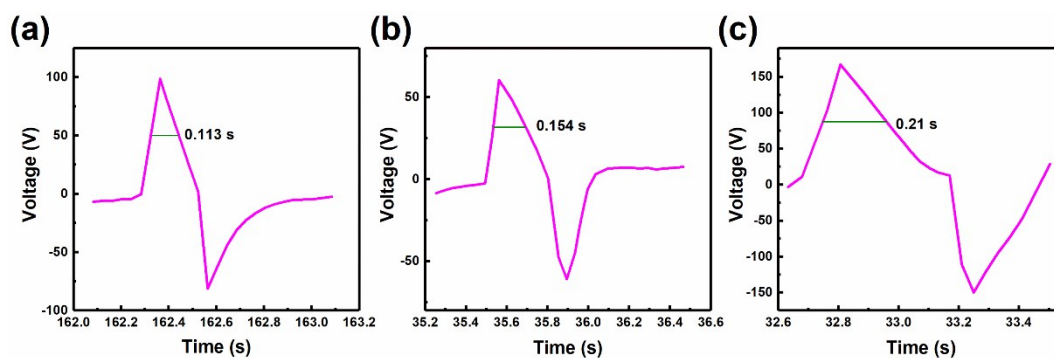


**Fig. S11** One pulse of voltage signal for the three modes: (a) PEH; (b) TEH; (c) P-TEH.

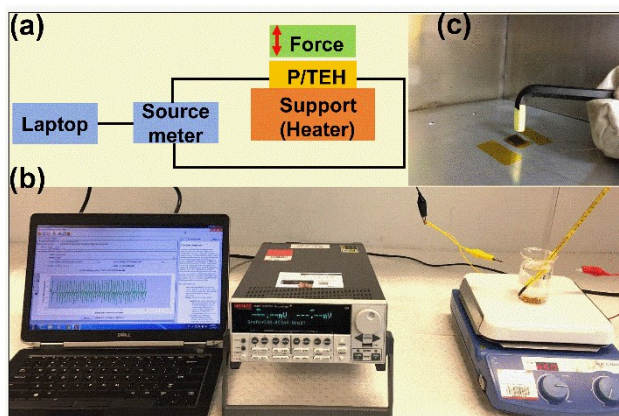


**Fig. S12** (a) Schematic diagram of the measurement system, picture of the high temperature measurement of (b) PEH in silicone oil and (c) P-TEH in oven.

## References

- 1 Y. H. Sun, J. G. Chen, X. N. Li, Y. Lu, S. J. Zhang, Z. X. Cheng, Flexible piezoelectric energy harvester/sensor with high voltage output over wide temperature range, *Nano Energy*, 2019, **61**, 337-345.
- 2 K. I. Park, M. Lee, Y. Liu, S. Moon, G. T. Hwang, G. Zhu, J. E. Kim, S. O. Kim, D. K. Kim, Z. L. Wang, K. J. Lee, Flexible nanocomposite generator made of BaTiO<sub>3</sub> nanoparticles and graphitic carbons, *Adv. Mater.*, 2012, **24**, 2999-3004.
- 3 S. Siddiqui, D. -I. Kim, M. T. Nguyen, S. Muhammad, W. -S. Yoon, N. -E. Lee, High-performance flexible lead-free nanocomposite piezoelectric nanogenerator for biomechanical energy harvesting and storage, *Nano Energy*, 2015, **15**, 177-185.
- 4 R. S. Yang, Y. Qin, C. Li, G. Zhu, Z. L. Wang, Converting biomechanical energy into electricity by a muscle-movement-driven nanogenerator, *Nano Lett.*, 2009, **9**, 1201-1205.